A global survey of cloud overlap based on CALIPSO and CloudSat measurements

Jiming Li,[1] Jianping Huang,[1,*] Knut Stamnes,[2]
Tianhe Wang,[1] Qiaoyi Lv[1], Hongchun Jin[1]

[1]Key Laboratory for Semi-Arid Climate Change of the Ministry of Education, College of Atmospheric Sciences, Lanzhou University, Lanzhou, China

[2]Department of Physics and Engineering Physics, Stevens Institute of Technology, Hoboken, NJ, USA

Running Head: Statistical properties of cloud overlap

*Corresponding author: Jianping Huang, Key Laboratory for Semi-Arid Climate Change of the Ministry of Education, College of Atmospheric Sciences, Lanzhou University, Lanzhou, Gansu 730000, China. (hjp@lzu.edu.cn)

Abstract

Using 2B-CLDCLASS-Lidar (Radar-Lidar) cloud classification and 2B-FLXHR-LIDAR radiation products from CloudSat over four years, this study evaluates the co-occurrence frequencies of different cloud types, analyzes their along-track horizontal scales and cloud radiative effects (CREs), and utilizes the vertical distributions of cloud types to evaluate cloud-overlap assumptions.

The statistical results show that high clouds, altostratus, altocumulus and cumulus tend to co-exist with other cloud types. However, stratus (or stratocumulus), nimbostratus and convective clouds are much more likely to exhibit individual features than other cloud types. On average, altostratus-over-stratus/stratocumulus cloud systems have a maximum horizontal scale (17.4 km), with a standard deviation of 23.5 km. altocumulus-over-cumulus has a minimum scale (2.8 km), with a standard deviation of 3.1 km. By considering the weight of each multilayered cloud type, we find that the global mean instantaneous net CREs of multilayered cloud systems during the daytime are approximately -41.3 W/m^2 and -50.2 W/m^2, which account for 40.1% and 42.3% of the global mean total net CREs at the top of the atmosphere (TOA) and at the surface, respectively. The radiative contributions of high-over-altocumulus and high-over-stratus/stratocumulus (or cumulus) in the all multilayered cloud systems are dominant due to their frequency.

Considering the overlap of cloud types, the cloud fraction based on the random overlap assumption is underestimated over vast oceans, except in the west-central Pacific Ocean warm pool. Obvious overestimations mainly occur over tropical and subtropical land masses. In view of an lower degree of overlap than that predicted by the random overlap assumption occur over the vast ocean, particularly poleward of 40 ℃S, the study therefore suggest that a linear combination of minimum and random overlap assumptions may further improve the predictions of actual cloud fractions for multilayered cloud types (e.g., As+St/Sc and Ac+St/Sc) over the Southern Ocean. The establishment of statistical relationship between multilayered cloud types and the environmental conditions (e.g., atmospheric vertical motion, convective stability and

wind shear) would be useful for parameterization design of cloud overlap in numerical models.

1. Introduction

As the most important regulators of the Earth's climate system, clouds significantly affect the radiation budget, the hydrological cycle and the large-scale circulation of the Earth (Hartmann et al., 1992; Stephens, 2005). However, because of incomplete knowledge of their underlying physical processes, clouds are still poorly represented in climate and weather models (Zhang et al., 2005) and are considered a major source of uncertainty in climate change predictions by GCMs (Cess et al., 1990).

Cloudiness is composed of a variety of types that are governed by different types of atmospheric motion and are associated with different microphysical properties; On the other hand, different cloud types have distinct cloud radiative effects and precipitation forms (Ackerman et al., 1988; Betts and Boers, 1990; Hartmann et al., 1992). However, multilayered cloud systems, in which two or more cloud types are simultaneously present over the same location but at different levels in the atmosphere, have been frequently reported by surface and aircraft observations (Tian and Curry, 1989). The frequent co-occurrences of different cloud types in the atmosphere increase the complexity of present cloud climatology studies. For example, the effects of individual cloud types on the surface and atmospheric radiation budgets depend on whether other clouds are also present above or below them. In addition, cloud overlap variations can significantly change atmospheric radiative heating/cooling rates, atmospheric temperatures, hydrological processes, and daily variability (Chen and Cotton, 1987; Morcrette and Jakob, 2000; Liang and Wu, 2005). Therefore, to improve radiation calculations of climate prediction models, understand cloud physical processes, and evaluate the schemes for generating clouds in those models, it is necessary to know the amount and distribution of each cloud type, particularly a detailed description of the co-occurrence of different cloud types and their statistical

properties.

Until recently, many related studies on cloud types and cloud overlap, which are based on several fundamentally different types of passive observational datasets (typically the International Satellite Cloud Climatology Project (ISCCP) and surface observer reports), have focused on the geographical distributions and long-term variations of cloud types (e.g., Rossow and Schiffer, 1991; Rossow and Schiffer,1999; Hahn et al., 2001; Warren et al., 2007; Eastman et al., 2011; Eastman et al., 2013), cloud radiative effects (Hartmann et al., 1992; Chen et al., 2000; Yu et al., 2004), cloud-property retrievals in multilayered clouds using multi-channel measurements from passive sensors (Chang and Li, 2005a, Chang and Li, 2005b; Huang et al., 2005; Huang et al., 2006a; Huang et al., 2006b; Minnis et al., 2007), and the statistics of cloud overlap based on surface weather reports and measurements from ground-based cloud radar (Warren et al., 1985; Hogan and Illingworth, 2000; Minnis et al., 2005). However, these studies have different limitations and uncertainties. First, passive detection methods and cloud-classification algorithms generally fail to detect multilayered clouds effectively. Such as, the existence of overlapping cloud layers may obscure the upper-level clouds from the perspective of a ground-based weather reporter, and lower clouds may be hidden from the view of a passive satellite. As a result, surface observer reports and ISCCP significantly underestimate high and low cloud frequencies, respectively, and introduce significant biases into the trend analysis of cloud cover, retrievals of cloud properties and evaluations of cloud radiative effects for the multilayered cloud systems since passive satellite retrieval techniques are based on the typical single-layered cloud assumption. Second, although the cloud properties can be retrieved relatively accurately from ground based lidar or radar signals, only one-dimensional observations are possible, and the sites are sparsely distributed, almost non-existent over the oceans. Third, most of these studies are limited to specific locations and time periods or specific multilayered (or single-layered) cloud systems. Systematic studies on the statistical co-occurrence of different cloud types on a global scale still have received far less attention.

Fortunately, the millimeter-wavelength cloud-profiling radar (CPR) on CloudSat

(Stephens et al., 2002) and the cloud-aerosol lidar with orthogonal polarization (CALIOP) (Winker et al., 2007) on CALIPSO (launched in late April 2006) provide an unprecedented opportunity for detailed studies on the three-dimensional structures of clouds on a global scale. Since mid-June 2006, CALIPSO and CloudSat data have been widely used to investigate the three-dimensional distributions and structures of hydrometeors and to improve the cloud-overlap assumption used in GCMs (e.g., Barker, 2008; Luo et al., 2009; Kato et al., 2010; Li et al., 2011). By using a radar-only cloud-classification product (i.e., the 2B-CLDCLASS dataset from CloudSat), Sassen and Wang (2008) presented the geographical distributions and global average frequency of each cloud type. In this study, we investigate the co-occurrence frequencies of different cloud types and analyze their along-track horizontal scales and radiative effects using the latest cloud-classification and radiative-flux products based on the combined measurements of the two active sensors mentioned previously. Finally, we perform a preliminary evaluation of how well cloud-overlap assumptions characterize the overlap of two apparently separate cloud types. Although some statistical results reasonably agree with previous studies, new insights are achieved in this investigation. These new results will hopefully be useful for future GCMs evaluations and improvements.

The study is organized as follows. The dataset for the research is described in Section 2. Section 3 provides the zonal distributions and global statistics of the co-occurrence frequencies of cloud types and discusses their along-track horizontal scales and radiative effects. An evaluation of the performance of cloud-overlap assumptions based on the co-occurrence frequencies of cloud types is presented in Section 4.

2. Data

In the following study, four years (2007-2010) of data from the latest release of the CloudSat 2B-CLDCLASS-Lidar (version 1.0) product (i.e., Radar-Lidar cloud classification) and the 2B-FLXHR-LIDAR product are collected to analyze cloud types and discuss their co-occurrence frequencies, horizontal scales and radiative effects.

The ISCCP uses a combination of cloud-top pressure and cloud optical depth to classify clouds into cumulus, stratocumulus, stratus, altocumulus, altostratus, nimbostratus, cirrus, cirrostratus, and deep convective clouds. However, traditional surface observations identify clouds by using basic features (e.g., base height, horizontal and vertical dimensions, and precipitation types) of the major cloud types (World Meteorological Organization, 1956; Parker, 1988; Moran et al., 1997). Based on these basic cloud characteristics, Wang and Sassen (2001) classified cloud types into eight classes by combining the range capabilities of active sensors (radar and lidar) and the auxiliary measurements from the other passive sensors (e.g., infrared and microwave radiometers); they further indicated the overall agreement (approximately 70%) between the results from their algorithm and the surface visual observations from the Southern Great Plains (SGP) CART site.

Based on the algorithm presented by Wang and Sassen (2001), the Radar-Lidar cloud classification identifies the cloud types using two steps. First, combined radar and lidar cloud-mask results are used to find a cloud cluster according to cloud persistence in the horizontal and vertical directions. By performing the cloud clustering analysis, a CloudSat granule may be divided into a number of cloud clusters, depending on the cloud systems present. Once a cloud cluster is found, the cloud height and phase, maximum effective radar reflectivity factor (Ze) and temperature, and the occurrence of precipitation are determined. Second, the cluster mean properties and spatial inhomogeneities, in terms of the cloud-top heights and maximum signals of the radar and lidar, are sent to a fuzzy classifier to classify the cluster into one cloud type with an assigned confidence level. To improve the classification flexibility, a combination of rule-based and fuzzy-logic-based classification is used in this algorithm. The cloud-phase determination is based on rules, and the cloud-type classification is mainly based on fuzzy logic (see Wang et al., Level 2 Combined Radar and Lidar Cloud Scenario Classification Product Process Description and Interface Control Document, version 1.0, 2013, available at http://www.cloudsat.cira.colostate.edu/dataSpecs.php?prodid=12&pvid=12). The cloud types provided by this product (version 1.0) include high clouds (High),

174 altostratus (As), altocumulus (Ac), stratus (St), stratocumulus (Sc), cumulus (Cu),
175 nimbostratus (Ns) and deep convective (Dc) clouds. The High cloud type includes
176 cirrus, cirrocumulus and cirrostratus, and the Cu cloud type represents cumulus
177 congestus and fair weather cumulus. Following the study of Sassen and Wang (2008),
178 we also combine two cloud types (St and Sc) into St+Sc in the present study. By
179 combining the unique complementary capabilities of the cloud profile radar (CPR) of
180 CloudSat and the space-based polarization lidar (CALIOP), some CPR weaknesses
181 (e.g., high surface contamination in the lowest three to four vertical bins of the CPR
182 and a lower sensitivity to optically thin clouds) are minimized in the latest
183 Radar-Lidar cloud classification product; thus, the identification of High (cirrus or
184 cirrostratus) and low cloud types (such as St, Sc and Cu) is significantly improved in
185 the 2B-CLDCLASS-Lidar product.

186 By using CloudSat microphysical retrievals, a combined CloudSat/CALIPSO
187 cloud mask and lidar-based aerosol retrievals as inputs for a broadband, two-stream,
188 plane-parallel, adding-and-doubling radiative transfer model, the 2B-FLXHR-LIDAR
189 product provides calculated radiative fluxes and atmospheric heating rates at 240 m
190 vertical increments (Henderson et al., 2013). Incorporating the radiative influence of
191 optically thin and low clouds that were undetected by CloudSat significantly
192 improved the agreement between the 2B-FLXHR-LIDAR calculations and
193 observations from the Clouds and the Earth's Radiant Energy System (CERES)
194 experiment. Henderson et al. (2013) showed that the global mean outgoing shortwave
195 radiation (OSR) and outgoing longwave radiation (OLR) estimated from the
196 collocated CERES observations and 2B-FLXHR-LIDAR calculations agree within 4
197 and 5 W/m^2, respectively, with root-mean-square differences of 6 W/m^2 and 16 W/m^2
198 on monthly/5 ° scales. Because the passive sensors largely fail to resolve the cloud
199 overlap in the vertical, the 2B-FLXHR-LIDAR product derived from these two active
200 sensors is considered a vital dataset for examining the radiative heating features in the
201 atmosphere and for studying the variations in fluxes and heating rate caused by
202 vertically overlapping clouds (L'Ecuyer et al., 2008; Haynes et al., 2013). In this
203 investigation, we only provide the results of the net radiative effect of different

multilayered cloud types at the TOA and at the surface during the daytime by using the 2B-FLXHR-LIDAR. However, it needs to further explain that the radiative effects of different cloud types only are the instantaneous effects at the overpass time of the satellites during the daytime in this study.

The following cloud parameters in the 2B-CLDCLASS-Lidar product are used in this study: cloud layer (CL) and cloud layer type (CLTY). In the 2B-FLXHR-LIDAR product, only the TOACRE (cloud radiative effect at the TOA) and BOACRE (cloud radiative effect at the surface) are used. Here, we consider one data profile as a multilayered (or single-layered) cloud profile when two or more cloud layers (or only one layer) are present within the vertical profile based on the parameter "cloud layer". To map the regional variability in the studied variable, we group the global area into $2°\times2°$ grid boxes to collect a sufficient number of samples in each grid box. Following the definitions of cloud fraction and cloud amount proposed by Hagihara et al. (2010), the cloud-type fractions and amounts in a given grid box are defined as the number of particular cloud-type profiles divided by the number of total sample profiles and the total cloud profiles within this box, respectively. For example, the cloud fraction for multilayered clouds is the ratio of the number of multilayered cloud profiles to the number of total sample profiles in a given grid box. In this investigation, we only provide the annual average cloud properties of different overlapping cloud types with small seasonal variations. In addition, comparisons of the four-year average cloud fractions for different cloud types between daytime and night-time are provided in tables. Notably, the day-night comparisons of cloud fractions are only represented by the two overpass times of the satellites. The full diurnal cycle cannot be captured by CALIPSO and CloudSat. Sassen et al. (2009) showed that the observed day-night variations in cirrus observed by CALIPSO mostly reflect real cloud processes, even when the strong solar noise signature impacts the comparisons of cloud types between day and night, particularly for cirrus. For other cloud types, the uncertainty caused by the daylight noise for lidar may be smaller. Thus, the calculated annual mean cloud fractions for different cloud types in this investigation are reliable.

3. Simultaneous co-occurrence of different cloud types

3.1. Zonal distributions of overlapping clouds

Multilayered cloud systems frequently occur in the atmosphere. Our statistical results show that the seasonal variations in multilayered cloud percentages are small, and the seasonal globally averaged values range between 25% and 28%. These results are comparable to the multilayered cloud fractions (approximately 27%) from the Geoscience Laser Altimeter System (GLAS) (Wylie et al., 2007). Furthermore, we plot the global and zonal distributions of the annually averaged multilayered cloud fractions (see Fig.1). In Fig.1a, the high-value and low-value centers of the multilayered cloud fractions are very obvious. For example, equatorial central South America, western Africa, Indonesia and the west-central Pacific Ocean warm pool are typical high-value centers. There are three obvious peaks in the zonal mean patterns (Fig.1b): one major peak occurs in the tropics, and two minor peaks occur in the midlatitudes; two local minima occur in the subtropics. The local maximum during spring (thick, black line) in the northern midlatitudes may be the result of misidentifying high-level dust transport as high ice clouds or the result of the actual influences of dust on ice nucleation (Chen et al., 2010; Yu et al., 2012; Yuan and Oreopoulos, 2013).

In all multilayered clouds, we further identify the most frequently multilayered cloud systems (annually) and provide their zonal distributions (Fig. 2). Note that the overlap of the same cloud type (e.g., High+High) is not important in numerical climate simulations because these clouds have similar cloud properties and temperatures. Thus, treating these clouds as a single layer may not introduce serious errors into the calculation of the cloud properties (Wang and Dessler, 2006). In addition, the overlap of specific two cloud types in any three or more layer cloud systems (e.g., High+As+Cu) is also included in statistical results of their occurrence frequencies. But, only two layer cloud systems is used when we calculate the weighted cloud radiative effect of specific two cloud types-overlap in section 3.3. Fig. 2 clearly indicates that the zonal patterns of different combinations of cloud types are very different. For example, multilayered cloud systems that include high clouds

either have one peak in the tropics (High+Ac and High+Cu) or three peaks in the tropics and midlatitudes (High+St/Sc, High+Ns and High+As). The high clouds that represent the major peak in the tropics may be caused by large-scale ascent or by dissipating deep convection. However, gentle large-scale ascent and ice cloud production within frontal convection are likely responsible for the two minor peaks of the multilayered cloud systems along midlatitude storm tracks. In addition to these combinations of cloud types, As-over-stratiform clouds or Ac-over-stratiform clouds also tend to be concentrated in the midlatitudes (60 º and poleward). In fact, the distributions of clouds in different geographical regimes depend on the large scale circulation, but the environmental factors in same regimes, such as sea surface temperature, lower tropospheric stability, and vertical velocity are also important to the occurrences of different cloud types (Klein and Hartmann, 1993; Norris and Leovy, 1994). By studying the relations between various cloud types and the sea surface temperature of the tropical oceans, Behrangi et al. (2012) indicated that as the SST increases, the fraction of multilayered clouds increases up to a SST of 303 K and then decreases for SSTs greater than 303 K. The ranges of SSTs are very different for different combinations of cloud types, e.g., high clouds over St/Sc or Ns clouds tend to occur between 292 and 294 K, but high clouds over Ac, As or Cu clouds tend to occur between 302 and 304 K, even though almost all of the clouds have major peak values in the tropics. In addition, Yuan and Oreopoulos (2013) indicated that the vertical velocity of large-scale pressure systems has a negative correlation with the percentage of multilayered cloud systems. Strong subsidence favors low cloud formation and suppresses ice cloud generation; thus, multilayered clouds are infrequent over major Sc-dominated oceanic areas at latitudes near 30 °.

However, multilayered cloud systems are very difficult to detect by passive satellites (such as ISCCP) and by surface weather reporters, particularly during the night-time and for cloud systems that include very thin cirrus (Sassen and Cho, 1992; Liao et al., 1995). For example, when a high-level transparent cirrus cloud overlies a boundary layer stratus cloud, the retrieved cloud-top heights typically lie between the cirrus and stratus cloud heights (e.g., Baum and Wielicki, 1994), leading to the

misinterpretation of cloud types by ISCCP. For cloud property retrievals, the influence of liquid water clouds and precipitation on the radiances observed at the TOA is also one of the greatest impediments to determining the cloud ice mass for multi-layered systems that include ice clouds above water clouds (Huang et al., 2006a).

3.2. Global statistics of cloud overlap

The global average percentage overlap of different combinations of cloud types over land or ocean during the daytime and night-time are provided in Tables 1 and 2, respectively. These tables show that high clouds, As, Ac and Cu tend to co-exist with other cloud types, regardless of the time of day or surface type. The frequency of High-over-Ac over ocean may even exceed the frequency of single-layered Ac clouds over ocean, indicating that these two types actually exhibit a stronger meteorological association. However, St/Sc and Ns are much more likely to exhibit individual features than other types, particularly St/Sc over the ocean. Convective clouds are also typically in single layers. Although Cu form in unstable air and As form in stable air, a small percentage of overlap occurs. Globally, 44% (50%) and 35% (39%) of low clouds (St/Sc +Cu) over land and ocean during the daytime (night-time) are overlapped by other cloud types aloft. Approximately 23% (26%) and 20% (25%) of low clouds over land and ocean during the daytime (night-time) are connected with high clouds. These percentages are comparable to those (approximately 30%) presented by Yuan and Oreopoulos (2013). Notably, high clouds also include cirrostratus and cirrocumulus; thus, the percentage of overlap of deep convection below high clouds is approximately 29%, which is larger than the percentage (approximately 24%) of cirrus-over-convection clouds based on ICESat/GLAS (Geoscience Laser Altimeter System) (Wang and Dessler, 2006).

Based on the above figures and tables, we plot the global distributions of the annual mean dominant cloud types and their cloud fractions. Here, the cloud types include all single-layered and multilayered cloud systems (see Fig. 3a-3b). Fig. 3c-3d shows that the global distributions of the annual mean cloud types (only for multiple dominant clouds) and corresponding cloud amounts. Based on Fig.3a-3b, St/Sc is the

dominant cloud type worldwide, particularly over the ocean. High clouds are mainly concentrated in the tropics and subtropics. In addition, over Antarctica, the most frequent cloud type is As. These results are in reasonable agreement with the findings based on the ISCCP D1 dataset (Doutriaux-Boucher and Seze, 1998). However, Fig. 3a-3b also shows that As prevails over the arid/semi-arid land in the Northern Hemisphere, such as northwestern China and North America. In contrast, Ac is dominant over the arid/semi-arid land of the Southern Hemisphere, such as Australia and southern Africa. However, not all of these features are observed by Doutriaux-Boucher and Seze (1998) using the ISCCP D1 dataset. In fact, the obvious regional and seasonal variations in Ac and As are possibly related to the frequency of dust activities (Choi et al., 2009). In addition, over some deserts (such as the Sahara Desert), the most prevalent cloud type is low-level clouds (St/Sc) according to the ISCCP D1, as opposed to the high clouds in our results. This discrepancy may be due to inadequate identification of airborne dust, such as the ISCCP misclassifying dust as low-level clouds, as suggested by the low values of the effective droplet radius reported by Han et al. (1994) over these regions.

Generally, the High-over-St/Sc and High-over-Cu cloud systems are more common over the vast oceans of the tropics and midlatitudes, while High-over-Ac cloud systems tend to exist over land at the same latitudes (see Fig. 3c). Notably, As-over-Cu only occurs over northwestern China. In addition, the As-over-St/Sc cloud systems are dominant in the high latitudes. Fig. 3d shows the multilayered cloud-type amount, defined as the ratio of the cloud fraction of one multilayered cloud combination to the cloud fraction of total multilayered cloud systems. In addition, we note that some multilayered cloud systems (High-over-St/Sc) exist over the major Sc-dominated oceanic areas, which are generally unfavorable for upper-level cloud formation due to persistent strong subsidence. The major source of high clouds is topography-driven gravity wave activity, advection from neighboring tropical convection centers, such as the Amazon Basin or the Congo Basin, or ascent associated with midlatitude fronts.

3.3. Along-track horizontal scales and radiative effects of cloud overlap

The horizontal scale of a multilayered cloud system along the CALIPSO/CloudSat track is determined by calculating the number of continuous profiles (N), in which each profile includes a vertical column with a particular combination of cloud types. Considering the 1.1 km along-track resolution of CPR measurements, the along-track scale (L in km) of a multilayered cloud system is $L = N \times 1.1$ (Zhang et al., 2014).

Fig. 4a-4d presents the zonal variation in the along-track horizontal scales of clouds in the multilayered cloud systems and their probability distribution functions (PDFs). As shown in Fig. 4a-4b, the High+St/Sc, As+St/Sc, High+Ns and High+Dc cloud systems have obvious zonal variations. High+St/Sc and As+St/Sc have minimum scales (approximately 10 km) in the tropics and maximum scales (up to 20 km) poleward of 40° (i.e., along the storm tracks). However, the along-track horizontal scales of High+Ns and High+Dc decrease from the tropics to the poles. The zonal variations in the scales of other clouds systems are small, particularly for High+Cu, As+Cu and Ac+Cu (approximately 3 km). We also provide the global average along-track horizontal scales and standard deviation (STD) of these cloud systems in Fig. 4c-4d. Generally, As+St/Sc has a maximum scale (17.4 km) and STD (23.5 km), while Ac+Cu has a minimum scale (2.8 km) and STD (3.1 km). The result which the standard deviations are larger than mean values of cloud scale, was also found in the study of Zhang et al. (2014). They showed that the global mean Ac along-track horizontal scale is 40.2 km, but the standard deviation reaches 52.3 km. It is clear that the along-track horizontal scales of these cloud systems all have considerable variations globally. By assuming a typical grid resolution of 1° in global climate models, we find that all multilayered cloud types cannot be resolved by global climate models. The multilayered cloud systems that include Cu (such as High+Cu, Ac+Cu and As+Cu) are not even captured by regional climate models with higher grid resolutions (approximately 15 km).

Furthermore, Fig. 5a-5b shows the zonal distributions of the instantaneous net TOA cloud radiative effects (CREs) of these multilayered cloud systems at overpass time of satellite during the daytime. In addition, we also provide the zonal distributions of weighted instantaneous net CREs by considering the frequency of

occurrence of each cloud type during the daytime only (Fig. 5c-5d). Although the zonal distributions of the net CREs for these cloud systems are similar, i.e., decrease from the tropics to high latitudes, the radiative effects can be grouped into several distinct classes. For example, middle-over-low (such as As+Sc/St and As+Cu) cloud systems have comparable radiative effects (maximum value of -300 W/m^2), while high-over-low (such as High+Sc/St and High+Cu) cloud systems have small radiative effects (maximum value of -150 W/m^2). By considering the weight of each multilayered cloud type, we find that their contributions to the cloud radiative effect of the whole multilayered cloud system are different (Fig. 5c-5d). In the tropics, High+Ac and High+Cu contribute -9 W/m^2 and -8 W/m^2, respectively, to the net radiative effects. Other cloud types have obvious zonal distributions, and their contributions range from 0 to -6 W/m^2. In mid-high latitudes, some mid-over-low (such as As+Sc/St) cloud systems are more important to the regional energy balance, particularly over the Southern Ocean regions. Similar to Fig. 5, Fig. 6 presents the surface-based results during the daytime. In summary, the trends are similar, but all cloud types have larger radiative effects at the surface than at the TOA; specifically, the effect is an obvious surface cooling. Clearly, the energy differences in the net cloud radiative effects between the surface and the TOA are persistent and may significantly change the atmospheric radiative heating/cooling rates and temperature. However, the zonal variations of the instantaneous net CREs in the atmosphere show that the radiative impacts are very distinct for the different multilayered cloud types (see Figure S1). Most of the multilayered cloud types heat atmosphere (their peak values range from 0.5 W/m^2 to 3 W/m^2) almost at all latitudes except As+Sc/St, Ac+Sc/St and High+Sc/St cloud systems, which cause a weak atmospheric cooling (peak value is approximately -1 W/m^2) at mid and high latitudes. In addition, statistical results also further show that the combined net CRE of the ten multilayered cloud types in the atmosphere decreases from the tropics to high latitudes, its value ranges from 13 W/m^2 (heating effect) to -3 W/m^2 (cooling effect).

Fig. 7a-7b shows the global mean instantaneous net radiative effects of the ten multilayered cloud systems range from -100 W/m^2 to -350 W/m^2, except for High+Dc

(the black dots are the mean values and the lines represent the standard deviation). In Fig. 7c-7d, the black bars represent the weighted global mean instantaneous net radiative effects of each cloud type at the TOA and surface. By combining the all single-layered and multilayered cloud systems, the global mean total net CREs are approximately -103.1 W/m^2 and -118.8 W/m^2 at the TOA and at the surface, respectively. The all multilayered cloud systems contribute approximately 40.1% (-41.3 W/m^2) and 42.3% (-50.2 W/m^2) to the global mean total net CREs at the TOA and at the surface, respectively. Clearly, the existence of a multilayered cloud system is important to Earth's radiative energy balance. A further analysis shows that all two-layered and three-layered (or more layers) cloud systems contribute approximately -27.2 W/m^2 (-33.1 W/m^2) and -14.1 W/m^2 (-17.1 W/m^2), respectively, to the total cloud radiative effects at the TOA (surface). However, the radiative effects of ten multilayered cloud types in our study are -22.7 W/m^2 and -27.1 W/m^2 at the TOA and at the surface (a contribution of 22%). High+Ac and High+Sc/St (or Cu) have relatively smaller effects than High+Dc and Ac+Sc/St (or Cu), but their contributions to the cloud radiative effect of the all multilayered cloud systems are highest because of their more frequent occurrence, larger weights (see the gray line in Fig. 7c-7d), and distribution from the tropics to the midlatitudes (Fig. 3). However, the other cloud types may be important to regional cloud radiative effects. For example, mid-to-upper level clouds frequently coexist with boundary layer clouds (e.g., As+St/Sc and High+St/Sc) over the Southern Ocean; thus, mid-atmosphere cloudiness is overestimated by ISCCP and is partially responsible for the TOA shortwave radiation bias in the climate models over this region (Haynes et al., 2011).

4. Evaluation of cloud-overlap assumptions based on cloud types

Based on the advantages of the two active sensors, we preliminarily evaluate how well the cloud-overlap assumptions can characterize the overlap of two apparently separate cloud types using the 2B-CLDCLASS-Lidar cloud type product. The cloud overlap assumption has been widely used to describe the actual vertical distribution of clouds and the parameterization of the total cloud fraction in a given model grid box. Several basic cloud-overlap assumptions have been proposed, such as

maximum, random, random-maximum and minimum overlaps (Hogan and Illingworth, 2000). The most common cloud-overlap scheme in current GCMs is called "random-maximum" overlap, which assumes that cloud layers separated by clear layers are randomly overlapped, while vertically continuous cloud layers have maximum overlap (Stephens et al., 2004). When the cloud fractions of the upper and lower layers are C_1 and C_2, the total cloud fractions of the two cloud layers based on the overlap assumptions are given by:

$$C_{random}=C_1+C_2-C_1\times C_2,$$

$$C_{max}=\max(C_1, C_2), \text{ and}$$

$$C_{min}=\min(1, C_1+C_2). \quad (1)$$

In addition, if we know the actual overlap fraction $C_{overlap}$, then the observed total cloud fraction C_{real} can be written as:

$$C_{real}=C_1+C_2-C_{overlap} \quad (2)$$

However, Hogan and Illingworth (2000) proposed a simpler and more useful expression for the degree of cloud-layer overlap (exponential random overlap). In the expression, the mean observed cloud fraction of two cloud layers can be determined by the linear combination of the maximum and random overlap in terms of an "overlap parameter" a,

$$C_{real}=a\times C_{max}+(1-a)\times C_{random} \quad (3)$$

Here, the overlap parameter a is considered a function of the layer separation, and related to the vertical resolution and the horizontal domain size. a=0 is random overlap and a=1 is the maximum overlap. As C_{real} increasingly departs from C_{max} (trending toward C_{min}), a becomes negative, indicating a tendency for an even lower degree of overlap than that predicted by the random overlap assumption. In fact, previous studies already have shown that cloud overlap parameter is sensitivity to spatial scale of GCMs grid box. For example, Hogan and Illingworth (2000) found that a tends to increase with decreasing spatial and temporal resolution (that is, with an increasing vertical and horizontal scale of GCMs), but one interesting finding is that, with a temporal resolution of 3 hour (that is, horizontal scale of 216 km in their study) and a level separation of between 6 and 8 km, a falls to -0.1. Mace et al. (2002)

also found an increase in a with decreasing temporal resolution at all sites but the southern Great Plain (SGP) site while they find a decrease in a with decreasing spatial resolution. However, Naud et al. (2008) found a decrease in a with increasing spatial resolution by analyzing the cloud overlap at SGP site for the winter months. These studies further implied that the degree of cloud overlap also may depend on the other factors, such as, atmospheric vertical motion, convective stability and wind shear in different seasons besides vertical resolution and the horizontal domain size (Mace et al., 2002; Naud et al., 2008). For example, vertically continuous clouds tend to be more maximally overlapped in the presence of vertical motion in midlatitudes and decreased convective stability in the Tropics. However, large wind shears were found to increase the randomness of the overlap, with overlap becoming less than random in some cases (a<0). What changes from one high to low horizontal resolution is actually the increase of number of samples, which in turn may affect the averaged values of the vertical velocity, convective stability and wind shear, thus further effect the way cloudy layers overlap.

Based on several months of data from ICESat/GLAS observations, Wang and Dessler (2006) showed that overlap differences between the observed and random overlaps exist when describing the actual overlap of two separated cloud types (vertical separation >0.5 km). However, the authors' work focused on the tropics and was limited to simple cloud classifications using space-based lidar. We expand the study by Wang and Dessler (2006) by employing a global-scale analysis and a more complete cloud classification; the overlap of two separate cloud types (here, vertical separation >0.24 km at least) in each combination of cloud types in each grid box is determined. Moreover, we evaluate the performances of the random overlap assumption and calculate the overlap parameter a for each multilayered cloud type in each 2 °×2 ° grid box.

We first group each multilayered cloud system. For example, for the all High+Cu multilayered cloud systems in the same 2 °×2 ° grid box, we consider two layers and group all high clouds into the upper layer and all cumulus clouds into the lower layer, regardless of the vertical separation between these two types and their heights. Then,

four possible values for the combined total cloud fraction of the two cloud types at different layers are calculated by assuming random overlap, maximum overlap, minimum overlap and actually observed overlap. Because random cloud overlap is considered a better characterization of cloud overlap behavior than minimum overlap and maximum overlap when two cloud layers separated by clear layers, we only provide the difference in the cloud fractions between random overlap and actually observed overlap. Finally, the overlap parameter *a* for each multilayer in each grid is calculated based on Eq. (3). Notably, because we do not group multilayered cloud types into multiple layers according to the vertical separation of two types, only one value for the overlap parameter *a* for each multilayered cloud system in each grid is obtained. *a* may be considered the mean value of all overlap parameters at different layer separations. Here, we define the relative difference (RD) between the random and actual overlap for one of the multilayered cloud types as:

$$RD=(C_{random}-C_{real})/C_{real} \quad (4)$$

In addition, the cumulative relative difference (CRD) between the random and actual overlap for all multilayered cloud types (here, 17 different combinations of different cloud types are considered) in each 2 °×2 °grid box is given by:

$$CRD=\sum_{i=1}^{17} RD^i \times w^i \qquad i=1, 2, 3 \ldots, 17 \quad (5)$$

Similar to the definition of CRD, we define the cumulative overlap parameter (COP) in each 2 °×2 °grid box as:

$$COP=\sum_{i=1}^{17} a^i \times w^i \qquad i=1, 2, 3 \ldots, 17 \quad (6)$$

where *w* is the weight coefficient for one multilayered cloud type in each 2 °×2 °grid box as follows:

$$w^i=f^i/\sum_{i=1}^{17} f^i \qquad i=1, 2, 3 \ldots, 17 \quad (7)$$

f is the cloud fraction of each multilayered cloud type in every grid box.

Fig. 8a-8b shows the zonal distributions of the relative differences between the random and actual overlap for ten of the main multilayered cloud types and the cumulative relative differences for all multilayered cloud types (gray line). The results show that differences exist, even though the random-cloud-overlap assumption is

thought to better describe cloud-overlap behavior than other schemes when the cloud layers appear to be separate. The cloud fractions based on the random-overlap assumption are underestimated for High+St/Sc, As+St/Sc and Ac+St/Sc at all latitudes; these differences can exceed -5%. The cloud fraction of the High-over-Ac system is overestimated at all latitudes. The peak values of the difference are mainly located in mid- and high- latitudes in both hemispheres and are up to 5%. For other types, the relative differences are smaller and change with latitude. In summary, the cumulative relative difference of all multilayered cloud types is small (gray lines), and almost values are negative at all latitudes. In Fig. 8c-8d, we further show the zonal distributions of the overlap parameter for ten of the main multilayered cloud types and the cumulative overlap parameter of all multilayered cloud types. Clearly, the overlap parameters for High+St/Sc, As+St/Sc and Ac+St/Sc at all latitudes are negative, indicating a C_{real} departure from C_{max} (trending toward C_{min}) and a tendency for an even lower degree of overlap than predicted by the random overlap assumption. Thus, the linear combination of maximum and random overlap assumptions is problematic due to the negative overlap parameters in those regions, where the three multilayered cloud types mentioned above are dominant, particularly over the major Sc-dominated oceanic areas. However, the overlap parameters are positive for High+Ns and High+Ac. Thus, C_{real} has a value between C_{max} and C_{random}, and the exponential random overlap can predict the actual overlap of these two types very well. These results are intuitive, as cloud types are governed by different types of atmospheric motion and state. The formation of cumuli-form clouds may be related to the strong ascent or convectively unstable which result in clouds that increase in height more quickly, and increasing the degree of overlap with other cloud types. However, random or minimum overlap occurs preferentially in regions of subsidence or convective stability (favors strati-form cloud). Therefore, it is not difficult to understand why the zonal distributions of cloud overlap parameters are very different for similar cloud overlap systems (e.g., middle-over-low). For example, the overlap parameters of As+St/Sc and Ac+St/Sc over the Southern Ocean are obviously distinct from As+Cu and Ac+Cu. In summary, the cumulative overlap parameters of all

563 multilayered cloud types (gray lines) are negative at nearly all latitudes. However, two
564 points still require further interpretation. First, the cumulative overlap parameters in
565 the tropics and in the Northern Hemisphere have small values (and possibly positive
566 values); thus, random overlap or exponential random overlap is representative of the
567 actual conditions. Second, in the Southern Hemisphere, the cumulative overlap
568 parameters trend toward C_{min}; thus, a better prediction using random overlap or
569 exponential random overlap is difficult. This finding partially explains why the
570 climate model errors in the TOA fluxes over the Southern Ocean are the largest
571 (Trenberth and Fasullo, 2010). Based on the global results from this study, we also
572 further support the findings of Naud et al. (2008) that factors such as dynamics could
573 be connected to the way cloudy layers overlap. As a result, we suggest that a linear
574 combination of minimum and random overlap assumptions may further improve the
575 predictions of real cloud fractions for the multilayered cloud types in the Southern
576 Hemisphere (e.g., As+St/Sc and Ac+St/Sc), particularly poleward of 40 °S over the
577 ocean. However, only three cloud types (e.g., low-level marine stratus, convective
578 cloud and layered cloud) are diagnosed by the cloud scheme in current GCMs. To be
579 useful for parameterization design, it is necessary for the overlap behavior we observe
580 to be related to quantities predicted by a GCM. In view of the cloud types are
581 governed by different types of atmospheric motion and state, we thus consider
582 environmental conditions related to cloud formation as a means to parameterize the
583 overlap characteristics in numerical models. But, before that, statistical connection
584 between multilayered cloud types and the environmental conditions should be
585 established in the future studies by using global cloud-overlap and meteorological
586 reanalysis datasets.

587 The global distributions and statistical results of the cumulative relative difference
588 and the cumulative overlap parameter for all multilayered cloud types are shown in
589 Fig. 9 and Tables 3 and 4, respectively. Fig. 9a shows the cumulative relative
590 difference, whereas Fig. 9b shows the cumulative overlap parameter. In Fig. 9a, we
591 find that the cloud fractions based on the random overlap assumption are
592 underestimated over the vast ocean, except over the west-central Pacific Ocean warm

pool. Obvious overestimations occur over tropical and subtropical land masses, particularly where low multilayered cloud fractions are found, such as in equatorial central South America, southern and northern Africa, Australia and the Antarctic. In these regions, the High-over-Ac system is the dominant multilayered cloud type. This pattern indicates that land surface effects may favor an exponential random overlap. In Fig. 9b, the distributions of the cumulative overlap parameter are similar to the results of the cumulative relative difference. Negative overlap parameters also occur over the vast ocean, except over the west-central Pacific Ocean warm pool. The typical negative high-value centers correspond to the major Sc-dominated oceanic areas very well. The positive overlap parameters are mostly located over tropical and subtropical land masses and Antarctica. Globally, by using random overlap, the overlap percentages are overestimated by 24%, 21.9%, 30% and 133.3% for High clouds over As, St/Sc clouds, Ns, and Ac over St/Sc clouds, respectively, over land during the daytime (Table 3). An overestimation also occurs for As over Cu and St/Sc clouds. However, the overlap of High clouds with Ac and Cu is underestimated by -32.6% and -25% over land during the daytime, respectively. Regardless of vertical separation of two types, the absolute errors of cloud-type fractions (See Tables 3 and 4) seem small for global mean, but we should recall the previous finding that a 4% increase in low cloud cover would be sufficient to offset the warming effect of a doubling of CO2 (Randall et al. 1984), therefore, these bias errors in cloud cover possible induce a substantial bias error in the regional radiation budget. The underestimations (or overestimations) of the cloud fraction by the random overlap assumption ultimately cause overestimations (or underestimations) of cloud radiative effects. Globally, the overestimations of the net cloud radiative effect are obvious for High+St/Sc and Ac+St/Sc (approximately 3.9 W/m^2 at the surface, about 3.3% of the mean cloud forcing), whereas the underestimations of the net cloud radiative effect are obvious for High+Ac and High+Cu (Table 3). Generally speaking, change in cloud forcing caused by these bias errors in cloud cover is about 11 W/m^2 at the surface, about 10% of the mean cloud radiative effect at the surface. Thus, if these bias errors in cloud cover codified in GCMs, could bias climate feedbacks resulting

623 from increasing trace gasses or natural variability.

624 **5. Summary and discussion**

625 Although cloud types and their co-occurrence variations are the most significant
626 components of the global climate system and cloud climatology studies, systematic
627 and global studies on statistical properties of clouds have not received much attention.
628 This study quantitatively evaluates the co-occurrence frequencies of different cloud
629 types, analyzes their along-track horizontal scales and radiative effects by using the
630 latest cloud classification (2B-CLDCLASS-Lidar) and radiative flux products
631 (2B-FLXHR-LIDAR) based on 4 years of combined measurements from CALIPSO
632 and CloudSat. We also preliminary evaluate cloud-overlap assumptions. Although
633 some statistical results reasonably agree with previous research, new insights are also
634 achieved in this paper.

635 The statistical results clearly show that High clouds, As, Ac and Cu tend to
636 co-exist with other cloud types. However, St/Sc, Ns and convective clouds are much
637 more likely to exhibit individual features than other cloud types. The zonal variations
638 in along-track horizontal scales are distinct for different multilayered cloud systems.
639 On average over the globe, As+St/Sc has a maximum scale (17.4 km) and STD (23.5
640 km), while Ac+Cu has a minimum scale (2.8 km) and STD (3.1 km). By considering
641 the weight of each multilayered cloud type, the global mean instantaneous net cloud
642 radiative effects of all multilayered cloud systems during the daytime are
643 approximately -41.3 W/m^2 and -50.2 W/m^2, which account for 40.1% and 42.3% of
644 the global mean total net CREs at the top of the atmosphere (TOA) and at the surface,
645 respectively. However, the net radiative effects of ten multilayered cloud types in our
646 study are -22.7 W/m^2 and -27.1 W/m^2 (a radiative contribution of 22%) at the TOA
647 and at the surface, respectively. High+Ac and High+Sc/St (or Cu) cloud systems
648 dominate the weighted global mean net CREs of multilayered cloud types because
649 they are most frequent.

650 Active sensors allow us to preliminarily evaluate how well the overlap
651 assumptions describe the actual overlap of two separate cloud types. In summary, the
652 cloud fractions based on the random overlap assumption are mainly underestimated

over the vast ocean, except over the west-central Pacific Ocean warm pool. Obvious overestimations occur over tropical and subtropical land masses, particularly in regions with low multilayered cloud fractions. These bias errors in cloud cover may induce a substantial bias error in the regional radiation budget. Globally, change in cloud forcing caused by these bias errors is about 11 W/m^2 at the surface, contributes an about 10% of the mean cloud radiative effect at the surface. Considering that negative overlap parameters occur over the vast ocean, particularly poleward of 40 °S, we suggest that a linear combination of minimum and random overlap assumptions may further improve the predictions of actual cloud fractions for multilayered cloud types (e.g., As+St/Sc and Ac+St/Sc) over the Southern Ocean. In fact, negative overlap parameters indicate that fractions of cloud overlap are overestimated by random overlap assumption at mid and high latitudes of two hemispheres, and a tendency for an even more minimal degree of overlap than that predicted by the random overlap assumption is exist over there. Due to passive sensors (such as, ISCCP) usually fail to detect effectively the cloud overlap, thus minimum overlap is what ISCCP or another passive sensor would observe. However, why do the active sensors in our results and previous studies (Hogan and Illingworth, 2000; Mace et al., 2002) also tend into this direction over those regions? The reason possible is as cloud features in one bigger grid box (here, 2 °×2 °) associated with vertical wind shears (or other dynamical factors in those regions) that are sloped in space to become more grouped together, thus trending toward increasing cloud cover over there. But, similar trend whether can be observed by active sensors in a smaller spatial scale (such as, 1 °×1 °) still needs to be confirmed in the future study by using this dataset. Generally speaking, this study further verifies that factors such as dynamics related to cloud formation could be connected to the way cloudy layers overlap. Therefore, we may consider environmental conditions as a means to parameterize the overlap characteristics in order to be useful for parameterization design in numerical models. In addition, the seasonal variations of cloud overlap also must be studied, as one would expect if cloud systems are driven by processes related to convection during the warm season and synoptic scale systems during winter (Mace et al., 2002).

683 Previous studies have quantitatively evaluated the global mean cloud fraction of
684 each cloud type using various datasets (such as ISCCP). However, we identify new
685 features that were not observed with the ISCCP D1 dataset (Doutriaux-Boucher and
686 Seze, 1998). For example, As and Ac prevail over the arid/semi-arid land of the
687 Northern Hemisphere (northwestern China and North America) and Southern
688 Hemisphere (Australia and southern Africa), respectively. Although the
689 representations and simulations of these mid-level clouds in global climate models are
690 poor and under-predicted (Zhang et al., 2005), the balance of phases for these
691 mixed-phase clouds (mid-level clouds) due to cloud-layer temperature or ice nuclei
692 (IN) changes will certainly have a potentially large radiative impact in local regions
693 (Sassen and Khvorostyanov, 2007). Thus, to quantify the feedback of an individual
694 cloud type in these regions and document the local cloud climatology, related studies
695 on mid-level clouds in these arid/semi-arid regions should focus on the impacts of
696 dust aerosols on radiative effects and "cold rain processes" (Huang et al., 2006c;
697 2006d; Su et al., 2008; Wang et al., 2010).
698
699 **Acknowledgments**. This research was supported jointly supported by the National
700 Basic Research Program of China under No. 2013CB955802, No. 2012CB955301,
701 the National Science Foundation of China under grant 41205015, the Developmental
702 Program of Changjiang Scholarship and Innovative Research Team (IRT1018), the
703 China 111 project (No. B13045) and the Fundamental Research Funds for the Central
704 Universities (lzujbky-2013-105). We also would like to thank the CALIPSO, and
705 CloudSat science teams for providing excellent and accessible data products that
706 made this study possible.
707
708 **References**
709 Ackerman, T. P., Liou, K.N., Valero, F. P. J., and Pfister, L.: Heating rates in tropical
710 anvils, J. Atmos. Sci., 45, 1606–1623, 1988.
711 Barker, H.W.: Overlap of fractional cloud for radiation calculations in GCMs: a
712 global analysis using CloudSat and CALIPSO data, J. Geophys. Res., 113,

713 D00A01, doi:10.1029/2007JD009677, 2008.
714 Baum, B. A. and Wielicki, B. A.: Cirrus Cloud Retrieval Using Infrared Sounding
715 Data: Multilevel Cloud Errors, J. Appl. Meteor., 33, 107–117, 1994.
716 Behrangi, A., Kubar, T., and Lambrigtsen, B. H.: Phenomenological Description of
717 Tropical Clouds Using CloudSat Cloud Classification, Mon. Weather. Rev., 140,
718 3235–3249, 2012.
719 Betts, A. K. and Boers, R.: A cloudiness transition in a marine boundary layer, J.
720 Atmos. Sci., 47, 1480–1497, 1990.
721 Cess, R. D., Potter, G. L., Blanchet, J. P., Boer, G. J., Del Genio, A. D., Déqué, M.,
722 Dymnikov, V., Galin, V., Gates, W. L., Ghan, S. J., Kiehl, J. T., Lacis, A. A., Le
723 Treut, H., Li, Z. X., Liang, X.Z., McAvaney, B. J., Meleshko, V. P., Mitchell, J.
724 F. B., Morcrette, J. J., Randall, D. A., Rikus, L., Roeckner, E., Royer, J. F.,
725 Schlese, U., Sheinin, D. A., Slingo, A., Sokolov, A. P., Taylor, K.E., Washington,
726 W. M., Wetherald, R. T., Yagai, I., and Zhang, M. H.: Intercomparison and
727 interpretation of climate feedback processes in 19 atmospheric general
728 circulation models, J. Geophys. Res., 95, 16601–16615, 1990.
729 Chang, F. L. and Li, Z.: A new method for detection of cirrus overlapping- low clouds
730 and determination of their optical properties, J. Atmos. Sci., 62, 3993–4009,
731 2005a.
732 Chang, F. L. and Li, Z.: A near global climatology of single-layer and overlapped
733 clouds and their optical properties retrieved from TERRA/MODIS data using a
734 new algorithm, J. Clim., 18, 4752–4771, 2005b.
735 Chen, B., Huang, J., Minnis, P., Hu, Y., Yi, Y., Liu, Z., Zhang, D., and Wang, X.:
736 Detection of dust aerosol by combining CALIPSO active lidar and passive IIR
737 measurements, Atmos. Chem. Phys., 10, 4241-4251, 2010.
738 Chen, C. and Cotton, W. R.: The physics of the marine stratocumulus- capped mixed
739 layer, J. Atmos. Sci., 44, 2951–2977, 1987.
740 Chen, T., Rossow, W. B., and Zhang, Y.: Radiative Effects of Cloud-Type Variations,
741 J. Clim., 13, 264–286, 2000.
742 Choi, Y.S., Lindzen, R.S., Ho, C.H., and Kim, J.: Space observations of cold-cloud

743 phase change, Proc. Natl Acad. Sci., 107, 11211–11216, 2010.
744 Doutriaux-Boucher, M. and Seze, G.: Significant changes between the ISCCP C and D
745 cloud climatologies, Geophys. Res. Lett., 25, 4193-4196, 1998.
746 Eastman, R. and Warren, S. G.: A 39-Yr Survey of Cloud Changes from Land Stations
747 Worldwide 1971–2009: Long-Term Trends, Relation to Aerosols, and Expansion
748 of the Tropical Belt, J. Clim., 26, 1286-1303, 2013.
749 Eastman, R., Warren, S. G., and Hahn, C. J.: Variations in Cloud Cover and Cloud
750 Types over the Ocean from Surface Observations, 1954–2008, J. Clim., 24,
751 5914–5934, doi: 10.1175/2011JCLI3972.1, 2011.
752 Hagihara, Y., Okamoto, H., and Yoshida, R.: Development of a combined
753 CloudSat/CALIPSO cloud mask to show global cloud distribution, J. Geophys.
754 Res., 115, D00H33, doi:10.1029/2009JD012344, 2010.
755 Hahn, C. J., Rossow, W. B., and Warren, S. G.: ISCCP Cloud Properties Associated
756 with Standard Cloud Types Identified in Individual Surface Observations, J.
757 Clim., 14, 11–28, 2001.
758 Han, Q., Rossow, W. B., and Lacis, A. A.: Near-global survey of effective droplet
759 radii in liquid water clouds using ISCCP data, J. Clim., 7, 465-497, 1994.
760 Hartmann, D. L., Ockert-Bell, M. E., and Michelsen, M.L.: The effect of cloud type
761 on Earth's energy balance: global analysis, J. Clim., 5, 1281–1304, 1992.
762 Haynes, J.M., Jakob, C., Rossow, W.B., Tselioudis, G., and Brown, J.: Major
763 Characteristics of Southern Ocean Cloud Regimes and Their Effects on the
764 Energy Budget, J. Clim., 24, 5061-5080. doi: 10.1175/2011JCLI4052.1, 2011.
765 Haynes, J.M., Vonder-Haar, T.H., L'Ecuyer, T., Henderson, D.: Radiative heating
766 characteristics of Earth's cloudy atmosphere from vertically resolved active
767 sensors, Geophys. Res. Lett., 40, 624–630, doi:10.1002/grl.50145, 2013.
768 Henderson, D.S., L'Ecuyer, T., Stephens, G., Partain, P., and Sekiguchi, M.: A
769 multi-sensor perspective on the radiative impacts of clouds and aerosols, J. Appl.
770 Meteorol. Climatol., 52, 853–871, doi: 10.1175/JAMC-D-12-025.1, 2013.
771 Hogan, R. J. and Illingworth, A. J.: Deriving cloud overlap statistics from radar, Q. J.
772 Roy. Meteor. Soc., 128, 2903–2909, 2000.

773 Huang, J.P.: Analysis of ice water path retrieval errors over tropical ocean,
774 Advances in Atmospheric Sciences, 23: 165-180, 2006a.
775 Huang, J. P., Minnis, P., and Lin, B.: Advanced retrievals of multilayered cloud
776 properties using multispectral measurements, J. Geophys. Res., 110, D15S18,
777 doi:10.1029/2004JD005101, 2005.
778 Huang, J. P., Minnis, P., and Lin, B.: Determination of ice water path in ice-
779 over-water cloud systems using combined MODIS and AMSR-E measurements,
780 Geophys. Res. Lett., 33, L21801, doi:10.1029/ 2006GL027038, 2006b.
781 Huang, J.P., Lin, B., Minnis, P., Wang, T., Wang, X., Hu, Y., Yi, Y., and Ayers, J.R.:
782 Satellite-based assessment of possible dust aerosols semi-direct effect on cloud
783 water path over East Asia, Geophys. Res. Lett., 33, L19802, doi:
784 10.1029/2006GL026561, 2006c.
785 Huang, J.P., Minnis, P., Lin, B., Wang, T., Yi, Y., Hu, Y., Sun-Mack, S., and Ayers,
786 K.: Possible influences of Asian dust aerosols on cloud properties and radiative
787 forcing observed from MODIS and CERES, Geophys. Res. Lett., 33, L06824,
788 doi: 10.1029/2005GL024724, 2006d.
789 Kato, S., Sun-Mack, S., Miller, W. F., Rose, F. G., Chen, Y., Minnis, P., and Wielicki,
790 B. A.: Relationships among cloud occurrence frequency, overlap, and effective
791 thickness derived from CALIPSO and CloudSat merged cloud vertical profiles, J.
792 Geophys. Res., 115, D00H28, doi:10.1029/2009JD012277, 2010.
793 Klein, S. A. and Hartmann, D. L.: The seasonal cycle of low stratiform clouds, J.
794 Clim., 6, 1588–1606, 1993.
795 L'Ecuyer, T.S., Wood, N., Haladay, T., and Stephens, G.L.: The impact of clouds on
796 atmospheric heating based on the R04 CloudSat fluxes and heating rate dataset, J.
797 Geophys. Res., 113, D00A15, doi:10.1029/2008JD009951, 2008.
798 Li, J., Yi, Y., Minnis, P., Huang, J., Yan, H., Ma, Y., Wang, W., and Ayers, k.:
799 Radiative effect differences between multi-layered and single-layer clouds
800 derived from CERES, CALIPSO, and CloudSat data, J. Quant. Spectrosc. Radiat.
801 Transf., 112, 361–375, 2011.
802 Liang, X.Z., and Wu, X.: Evaluation of a GCM subgrid cloudradiation interaction

parameterization using cloud-resolving model simulations, Geophys. Res. Lett., 32, L06801, doi:10.1029/2004 GL022301, 2005.

Liao, X., Rossow, W. B., and Rind, D.: Comparison between SAGE II and ISCCP high-level clouds. Part I: Global and zonal mean cloud amounts, J. Geophys. Res., 100, 1121–1135, 1995.

Luo, Y., Zhang, R., and Wang, H.: Comparing occurrences and vertical structures of hydrometeors between the eastern China and the Indian monsoon region using CloudSat/CALIPSO data, J. Clim., 22, 1052-1064, 2009.

Mace, G. G., and Benson-Troth, S.: Cloud-layer overlap characteristics derived from long-term cloud radar data, J. Clim., 15, 2505–2515, 2002.

Minnis, P., Yi, Y., Huang, J., and Ayers, J. K.: Relationships between radiosonde and RUC-2 meteorological conditions and cloud occurrence determined from ARM data, J. Geophys. Res., 110, D23204, doi:10.1029/2005JD006005, 2005.

Minnis, P., Huang, J., Lin, B., Yi, Y., Arduim, R., Fan, T.-F., Ayers, J. K., and Mace, G. G.: Ice cloud properties in ice-over-water cloud systems using Tropical Rainfall Measuring Mission (TRMM) visible and infrared scanner and TRMM Microwave Imager data, J. Geophys. Res., 112, D06206, doi: 10.1029/2006JD007626, 2007.

Moran, J.M., Morgan, M.D., and Pauley, P.M.: *Meteorology: The Atmosphere and the Science of Weather*, Prentice Hall, New Jersey, 530pp, 1997.

Morcrette, J. J. and Jakob, C.: The response of the ECMWF model to changes in the cloud overlap assumption, Mon. Weather. Rev., 128, 1707–1732, 2000.

Naud, C.M., DelGenio, A.D., Mace, G.G., Benson, S., Clothiaux, E.E., and Kollias, P.: Impact of dynamics and atmospheric state on cloud vertical overlap, J. Clim., 21, 1758–1770, 2008.

Norris, J. R. and Leovy, C. B.: Interannual variability in stratiform cloudiness and sea surface temperature, J. Clim., 7, 1915–1925, 1994.

Parker, S.P.: *Meteorology Source Book*. McGraw-Hill, New York, 304 pp, 1988.

Randall, D.A., Coakley, Jr. J.A., Fairall, C.W., Kropfli, R.A., and Lenschow, D.H.: Outlook for research on sub-tropical marine stratiform clouds, Bull. Amer.

833 Meteorol. Soc., 65, 1290–1301, 1984.
834 Rossow, W. B. and Schiffer, R. A.: ISCCP cloud data products, B. Am. Meteorol.
835 Soc., 72, 2–20, 1991.
836 Rossow, W. B. and Schiffer, R. A.: Advances in understanding clouds from ISCCP, B.
837 Am. Meteorol. Soc., 80, 2261– 2286, 1999.
838 Sassen, K. and Cho, B. S.: Subvisual–thin cirrus lidar dataset for satellite verification
839 and climatological research, J. Appl. Meteor., 31, 1275–1285, 1992.
840 Sassen, K., and Khvorostyanov, V.I.: Microphysical and radiative properties of mixed
841 phase altocumulus: a model evaluation of glaciation effects. Atmos. Res., 84,
842 390–398, 2007.
843 Sassen, K. and Wang, Z.: Classifying clouds around the globe with the CloudSat radar:
844 1-year of results, Geophys. Res. Lett., 35, L04805, doi:10.1029/2007GL032591,
845 2008.
846 Sassen, K., Wang, Z., and Liu, D.: Cirrus clouds and deep convection in the tropics:
847 Insights from CALIPSO and CloudSat, J. Geophys. Res., 114, D00H06,
848 doi:10.1029/2009JD011916, 2009.
849 Stephens, G. L.: Cloud feedbacks in the climate system: a critical review, J. Clim., 18,
850 237–273, 2005.
851 Stephens, G. L., Wood, N. B., and Gabriel, P. M.: An assessment of the
852 parameterization of subgrid-scale cloud effects on radiative transfer: Part I.
853 Vertical overlap, J. Atmos. Sci., 61, 715–732, 2004.
854 Stephens, G.L., Vane, D.G., Boain, R.J., Mace, G.G., Sassen, K., Wang, Z.,
855 Illingworth, A.J., O'Connor, E.J., Rossow, W.B., Durden, S.L., Miller, S.D.,
856 Austin, R.T., Benedetti, A., Mitrescu, C., and CloudSat Science Team.: The
857 CloudSat mission and the A-Train, A new dimension of space-based
858 observations of clouds and precipitation, B. Am. Meteorol. Soc., 83,
859 1771–1790, 2002.
860 Su, J., Huang, J., Fu, Q., Minnis, P., Ge, J., and Bi, J.: Estimation of Asian dust
861 aerosol effect on cloud radiation forcing using Fu-Liou radiative model and
862 CERES measurements, Atmos. Chem. Phys., 8, 2763-2771, 2008.

863 Tian, L. and Curry, J. A.: Cloud overlap statistics, J. Geophys. Res., 94, 9925−9935,
864 1989.
865 Trenberth, K.E., and Fasullo, J.T.: Simulation of present-day and twenty-first-century
866 energy budgets of the southern oceans, J. Clim., 23, 440–454, 2010.
867 Wang, L. and Dessler, A. E.: Instantaneous cloud overlap statistics in the tropical area
868 revealed by ICESat/GLAS data, Geophys. Res. Lett., 33, L15804,
869 doi:10.1029/2005GL024350, 2006.
870 Wang, Z. and Sassen, K.: Cloud type and macrophysical property retrieval using
871 multiple remote sensors, J. Appl. Meteor., 40, 1665–1682, 2001.
872 Wang, W., Huang, J., Minnis, P., Hu, Y., Li, J., Huang, Z., Ayers, J. K., and Wang, T.:
873 Dusty cloud properties and radiative forcing over dust source and downwind
874 regions derived from A-Train data during the Pacific Dust Experiment, J.
875 Geophys. Res., 115, D00H35, doi: 10.1029/2010JD014109, 2010.
876 Warren, S. G., Eastman, R. M., and Hahn, C. J.: A survey of changes in cloud cover
877 and cloud types over land from surface observations, 1971–96, J. Clim., 20,
878 717–738, 2007.
879 Warren, S. G., Hahn, C. J., and London, J.: Simultaneous occurrence of different cloud
880 types, J. Clim. Appl. Meteorol., 24, 658–67, 1985.
881 Winker D. M., Hunt, W. H., and Mcgill, M. J.: Initial performance assessment of
882 CALIOP, Geophys. Res. Lett., 34, L19803, doi:10.1029/ 2007GL030135, 2007.
883 World Meteorological Organization.: *International Cloud Atlas: Abridged atlas*,
884 World Meteorological Organization, 62 pp., and 72 plates, Geneva, 1956.
885 Wylie, D.P., Eloranta, E., Spinhirne, J.D., and Palm, S.P.: A comparison of cloud
886 cover statistics from the GLAS lidar with HIRS, J. Clim., 20, 4968–4981,
887 doi:10.1175/JCLI4269.1, 2007.
888 Yu, R. C., Wang, B., and Zhou, T.: Climate effects of the deep continental stratus
889 clouds generated by the Tibetan Plateau, J. Clim., 17, 2702-2713, 2004.
890 Yu, H., Remer, L. A., Chin, M., Bian, H., Tan, Q., Yuan, T., and Zhang, Y.: Aerosols
891 from overseas rival domestic emissions over North America, Science, 337(6094),
892 566–569, doi:10.1126/science.1217576, 2012.

Yuan, T. and Oreopoulos, L.: On the global character of overlap between low and high clouds, Geophys. Res. Lett., 40, 5320–5326, doi:10.1002/grl.50871, 2013.

Zhang, D., Luo, T., Liu, D., and Wang, Z.: Spatial Scales of Altocumulus Clouds Observed with Collocated CALIPSO and CloudSat Measurements, Atmos. Res., 148, 58-69, doi: 10.1016/j.atmosres.2014.05.023, 2014.

Zhang, M. H., Lin, W. Y., Klein, S. A., Bacmeister, J. T., Bony, S., Cederwall, R. T., Del Genio, A.D., Hack, J. J., Loeb, N. G., Lohmann, U., Minnis, P., Musat, I., Pincus, R., Stier, P., Suarez,M. J., Webb, M. J., Wu, J. B., Xie, S. C., Yao, M. S., and Zhang, J. H.: Comparing clouds and 15 their seasonal variations in 10 atmospheric general circulation models with satellite measurements, J. Geophys. Res., 110, D15S02, doi:10.1029/2004JD005021, 2005.

Table 1. Globally averaged overlapping percentages of different cloud types over land and ocean during daytime.

	SL[a]	ML[b]	High	As	Ac	St/Sc	Cu	Ns	Deep	surface
High	8.8	14.5	3.7	2.5	4.3	3.2	2.8	1.0	0.4	Land
	8.8	**16.4**	**4.1**	**2.2**	**3.5**	**5.2**	**3.5**	**1.2**	**0.3**	**Ocean**
As	6.5	6.7	--	0.9	1.0	2.0	1.1	0.4	--	Land
	4.2	**6.1**	**--**	**0.5**	**0.9**	**2.5**	**1.0**	**0.3**	--	**Ocean**
Ac	5.3	7.0	--	0.01	1.1	0.9	1.1	0.04	--	Land
	3.1	**6.4**	**--**	**0.01**	**0.8**	**1.5**	**1.0**	**0.08**	--	**Ocean**
St/Sc	10.5	6.2	--	--	--	0.3	0.5	--	--	Land
	21.9	**9.4**	**--**	**--**	**--**	**0.4**	**0.7**	**--**	**--**	**Ocean**
Cu	3.9	5.1	--	--	--	0.1	0.3	--	--	Land
	6.6	**5.9**	**--**	**--**	**--**	**0.2**	**0.3**	**--**	**--**	**Ocean**
Ns	4.0	1.5	--	--	--	0.02	0.09	--	--	Land
	4.1	**1.6**	**--**	**--**	**--**	**0.02**	**0.05**	**--**	**--**	**Ocean**
Deep	0.8	0.4	--	--	--	--	--	--	--	Land
	0.8	**0.3**	**--**	**--**	**--**	**--**	**--**	**--**	**--**	**Ocean**

[a]The SL represents the single-layered cloud. [b]The ML represents the multi-layered cloud. And, those boldfaced values indicated the overlapping percentages of different cloud types over ocean.

Table 2. Globally averaged overlapping percentages for different cloud types over land and ocean during nighttime.

	SL[a]	ML[b]	High	As	Ac	St/Sc	Cu	Ns	Deep	surface
High	12.0	17.4	5.5	3.2	6.6	2.6	1.8	1.3	0.3	Land
	8.8	**20.8**	**4.7**	**2.3**	**5.0**	**7.6**	**4.4**	**1.3**	**0.3**	**Ocean**
As	6.9	7.4	--	1.0	1.1	1.9	0.9	0.4	--	Land
	3.9	**6.3**	**--**	**0.4**	**0.9**	**2.6**	**1.0**	**0.3**	--	**Ocean**
Ac	4.6	8.5	--	0.01	1.2	0.7	0.6	0.05	--	Land
	3.1	**8.1**	**--**	**0.01**	**1.0**	**1.9**	**1.2**	**0.08**	--	**Ocean**
St/Sc	6.4	5.1	--	--	--	0.2	0.3	--	--	Land
	23.8	**12.1**	**--**	**--**	**--**	**0.4**	**0.8**	**--**	**--**	**Ocean**
Cu	2.0	3.4	--	--	--	0.1	0.2	--	--	Land
	5.9	**6.9**	**--**	**--**	**--**	**0.2**	**0.4**	**--**	**--**	**Ocean**
Ns	3.9	1.7	--	--	--	--	0.08	--	--	Land
	4.0	**1.7**	**--**	**--**	**--**	**--**	**0.05**	**--**	**--**	**Ocean**
Deep	0.8	0.3	--	--	--	--	--	--	--	Land
	0.9	**0.3**	**--**	**--**	**--**	**--**	**--**	**--**	**--**	**Ocean**

[a]The SL represents the single-layered cloud. [b]The ML represents the multi-layered cloud. And, those boldfaced values indicated the overlapping percentages of different cloud types over ocean.

Table 3. Cloud fractions of different multilayered cloud types based on different overlap assumptions and observations during daytime. Here, $C_{overlap}$ and $C_1 \times C_2$ are the overlap cloud fraction from observations and overlap assumptions. "*a*" presents the overlap parameter.

Cloud type	C_{max}	C_{random}	C_{real}	$C_1 \times C_2$	$C_{overlap}$	R^a (W/m^2)	Diff.[b]	*a*
High+As	23.3	33.4	34.0	3.1	2.5	0.8	24.0%	-0.06
	(25.2)	**(32.9)**	**(33.3)**	**(2.6)**	**(2.2)**	**(0.8)**	**(18.2%)**	**(-0.05)**
High+Ac	23.3	32.7	31.3	2.9	4.3	-2.4	-32.6%	0.15
	(25.2)	**(32.3)**	**(31.2)**	**(2.4)**	**(3.5)**	**(-2.3)**	**(-31.4%)**	**(0.15)**
High+St/Sc	23.3	36.1	36.8	3.9	3.2	1.0	21.9%	-0.05
	(31.3)	**(48.6)**	**(51.3)**	**(7.9)**	**(5.2)**	**(3.9)**	**(51.9%)**	**(-0.16)**
High+Cu	23.3	30.2	29.5	2.1	2.8	-1.3	-25.0%	0.1
	(25.2)	**(34.5)**	**(34.2)**	**(3.2)**	**(3.5)**	**(-0.7)**	**(-8.6%)**	**(0.03)**
High+Ns	23.3	27.5	27.8	1.3	1.0	0.7	30.0%	-0.07
	(25.2)	**(29.5)**	**(29.7)**	**(1.4)**	**(1.2)**	**(0.5)**	**(16.7%)**	**(-0.05)**
High+Deep	23.3	24.2	24.1	0.3	0.4	-0.1	-25.0%	0.11
	(25.2)	**(26.0)**	**(26.0)**	**(0.3)**	**(0.3)**	**(0.0)**	**(0.0%)**	**(0.0)**
As+St/Sc	16.7	27.7	27.9	2.2	2.0	0.6	10.0%	-0.02
	(31.3)	**(38.4)**	**(39.1)**	**(3.2)**	**(2.5)**	**(2.5)**	**(28.0%)**	**(-0.1)**
As+Cu	13.2	21.0	21.1	1.2	1.1	0.4	9.1%	-0.01
	(12.5)	**(21.5)**	**(21.8)**	**(1.3)**	**(1.0)**	**(1.7)**	**(30.0%)**	**(-0.03)**
Ac+St/Sc	16.7	26.9	28.1	2.1	0.9	2.2	133.3%	-0.12
	(31.3)	**(37.8)**	**(39.3)**	**(3.0)**	**(1.5)**	**(3.9)**	**(100.0%)**	**(-0.23)**
Ac+Cu	12.3	20.2	20.2	1.1	1.1	0.0	0.0%	0.0
	(12.5)	**(20.8)**	**(21.0)**	**(1.2)**	**(1.0)**	**(0.5)**	**(20.0%)**	**(-0.02)**

[a]Calculated from (C_{random}-C_{real})×(global mean net cloud radiative effect of each cloud type). [b]Calculated from ($C_1 \times C_2$-$C_{overlap}$)/ $C_{overlap}$. And, those boldfaced values in the brackets indicated the overlapping percentages of different cloud types over ocean surface. But for R^a, the values indicated the net cloud radiative effect difference between real and random overlap at TOA and Surface (in the brackets), respectively. Here, only cloud radiative effects during daytime are considered.

Table 4. Cloud fractions of different multilayered cloud types based on different overlap assumptions and observations during nighttime. Here, $C_{overlap}$ and $C_1 \times C_2$ are the overlap cloud fraction from observations and overlap assumptions. "*a*" presents the overlap parameter.

Cloud type	C_{max}	C_{random}	C_{real}	$C_1 \times C_2$	$C_{overlap}$	R^a(W/m^2)	Diff.[b]	*a*
High+As	29.4	39.5	40.5	4.2	3.2	-	31.3%	-0.1
	(29.6)	**(36.8)**	**(37.5)**	**(3.0)**	**(2.3)**	-	**(30.4%)**	**(-0.1)**
High+Ac	29.4	38.6	35.9	3.9	6.6	-	-40.9%	0.29
	(29.6)	**(37.5)**	**(35.8)**	**(3.3)**	**(5.0)**	-	**(-34.0%)**	**(0.22)**
High+St/Sc	29.4	37.5	38.3	3.4	2.6	-	30.8%	-0.1
	(35.9)	**(54.9)**	**(57.9)**	**(10.6)**	**(7.6)**	-	**(39.5%)**	**(-0.16)**
High+Cu	29.4	33.2	33.0	1.6	1.8	-	-11.1%	0.05
	(29.6)	**(38.6)**	**(38.0)**	**(3.8)**	**(4.4)**	-	**(-13.6%)**	**(0.07)**
High+Ns	29.4	33.4	33.7	1.6	1.3	-	23.1%	-0.08
	(29.6)	**(33.6)**	**(34.0)**	**(1.7)**	**(1.3)**	-	**(30.8%)**	**(-0.1)**
High+Deep	29.4	30.2	30.2	0.3	0.3	-	0.0%	0.0
	(29.6)	**(30.4)**	**(30.5)**	**(0.4)**	**(0.3)**	-	**(33.3%)**	**(-0.13)**
As+St/Sc	14.3	24.2	23.9	1.6	1.9	-	-15.8%	0.03
	(35.9)	**(42.4)**	**(43.5)**	**(3.7)**	**(2.6)**	-	**(42.3%)**	**(-0.17)**
As+Cu	14.3	18.9	18.8	0.8	0.9	-	-11.1%	0.02
	(12.8)	**(21.7)**	**(22.0)**	**(1.3)**	**(1.0)**	-	**(30.0%)**	**(-0.03)**
Ac+St/Sc	13.1	23.1	23.9	1.5	0.7	-	114.3%	-0.08
	(35.9)	**(43.1)**	**(45.2)**	**(4.0)**	**(1.9)**	-	**(110.5%)**	**(-0.29)**
Ac+Cu	13.1	17.8	17.9	0.7	0.6	-	16.7%	-0.02
	(12.8)	**(22.6)**	**(22.8)**	**(1.4)**	**(1.2)**	-	**(16.7%)**	**(-0.02)**

[a]Calculated from (C_{random}-C_{real})×(global mean net cloud radiative effect of each cloud type). [b]Calculated from ($C_1 \times C_2$-$C_{overlap}$)/ $C_{overlap}$. And, those boldfaced values in the brackets indicated the overlapping percentages of different cloud types over ocean surface. But for R^a, the values indicated the net cloud radiative effect difference between real and random overlap at TOA and Surface (in the brackets), respectively. Here, only cloud radiative effects during daytime are considered.

Figure captions

Figure 1. (a) The global distribution ($2^{\circ}\times2^{\circ}$ grid boxes) of annually averaged multilayered cloud fraction. (b) The zonal distributions of seasonal averaged multilayered cloud fraction.

Figure 2. Zonal distributions of annual most frequently occurring multilayered cloud types based on the 2B-CLDCLASS-Lidar product.

Figure 3. The global distributions of (a) the annual mean dominant cloud types and (b) the corresponding cloud fractions. And, the global distributions of (c) the annual mean dominant multiple cloud types and (d) the corresponding cloud amounts.

Figure 4. (a)-(b):The zonal variation of cloud along-track horizontal scales for these multilayered cloud systems and (c)-(d): their probability distribution.

Figure 5. (a)-(d):The zonal distributions of instantaneous net cloud radiative effect and weighted instantaneous net cloud radiative effect by considering the frequency of occurrence of each cloud type for different multilayered cloud systems at the top of atmosphere (TOA) during daytime (that is, overpass time of satellite).

Figure 6. Same with Figure5, but at the surface during the daytime.

Figure 7. The global average instantaneous net cloud radiative effect and weighted instantaneous net cloud radiative effect for different multilayered cloud types at TOA and surface only during daytime. The gray line presents the global average frequency of occurrence of each cloud type only during daytime (that is, weights). The total weighted instantaneous net cloud radiative effects of ten multilayered cloud system are also showed in the figure 7c and 7d. TOA (-22.7 W/m^2); Surface (-27.1 W/m^2).

Figure 8. (a)-(b): The zonal distributions of the relative difference between the random and actual overlap for different multilayered cloud types and the cumulative relative difference of all multilayered cloud types (gray line). (c)-(d): The zonal distributions of the overlap parameter for different multilayered cloud types and the cumulative overlap parameter of all multilayered cloud types (gray line).

Figure 9. The global distributions of (a) the cumulative relative difference and (b) the

cumulative overlap parameter of all multilayered cloud types.

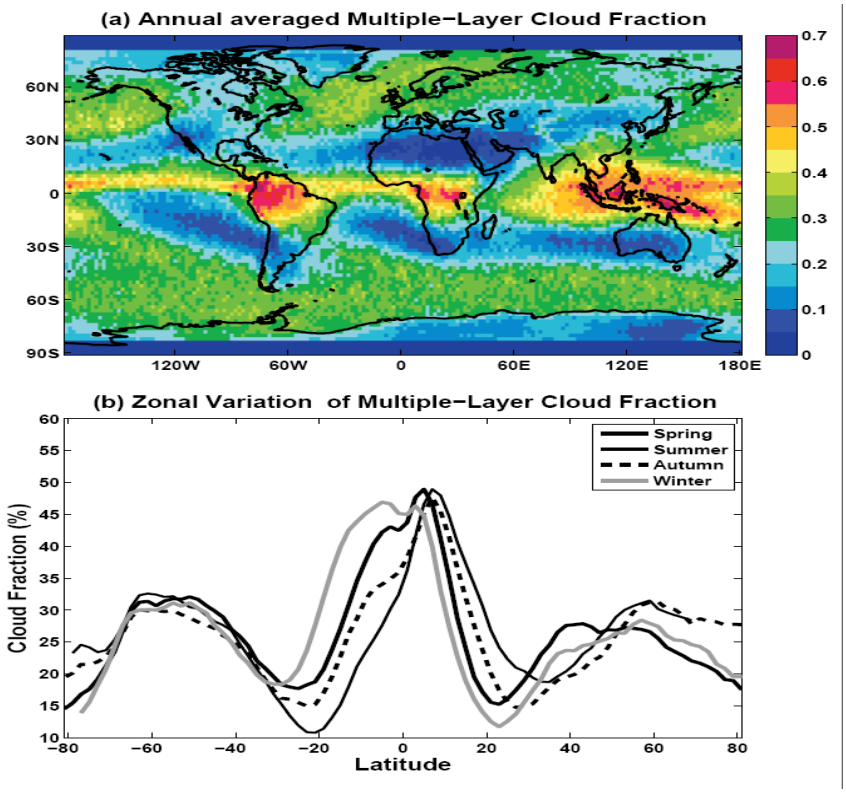

Figure 1. (a) The global distribution ($2^{\circ}\times2^{\circ}$ grid boxes) of annually averaged multilayered cloud fraction. (b) The zonal distributions of seasonal averaged multilayered cloud fraction.

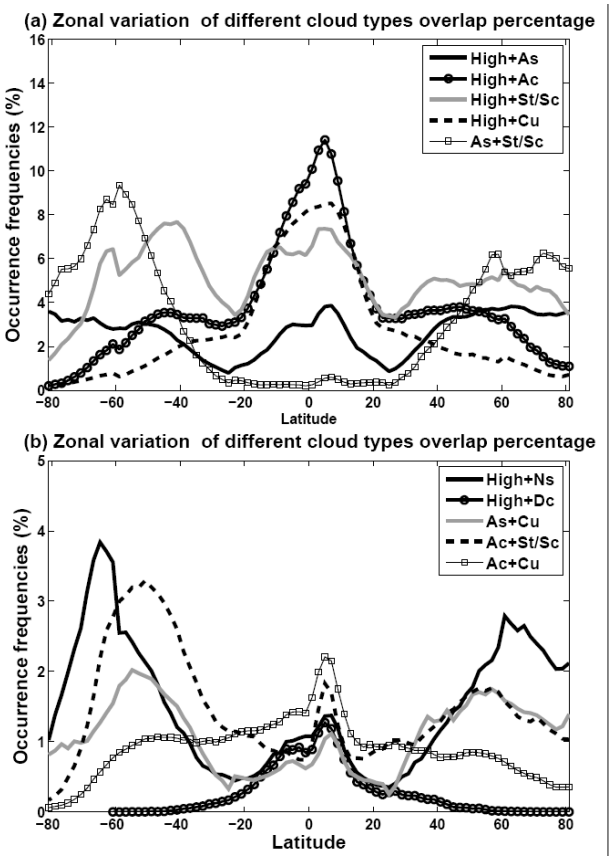

Figure 2. Zonal distributions of annual most frequently occurring multilayered cloud types based on the 2B-CLDCLASS-Lidar product.

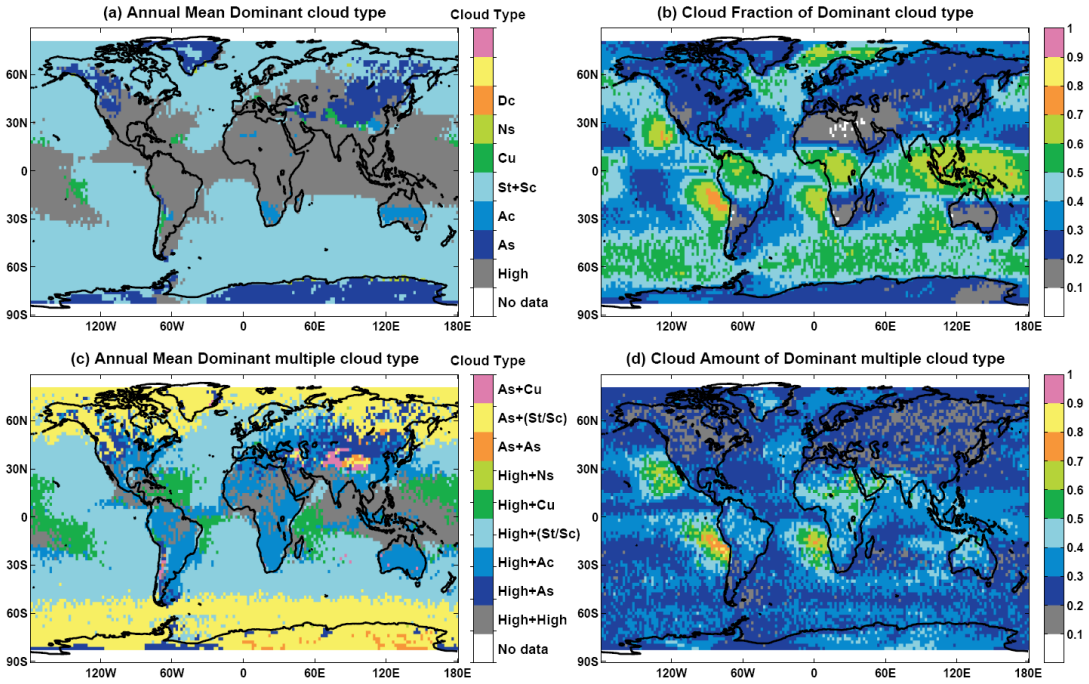

Figure 3. The global distributions of (a) the annual mean dominant cloud types and (b) the corresponding cloud fractions. And, the global distributions of (c) the annual mean dominant multiple cloud types and (d) the corresponding cloud amounts.

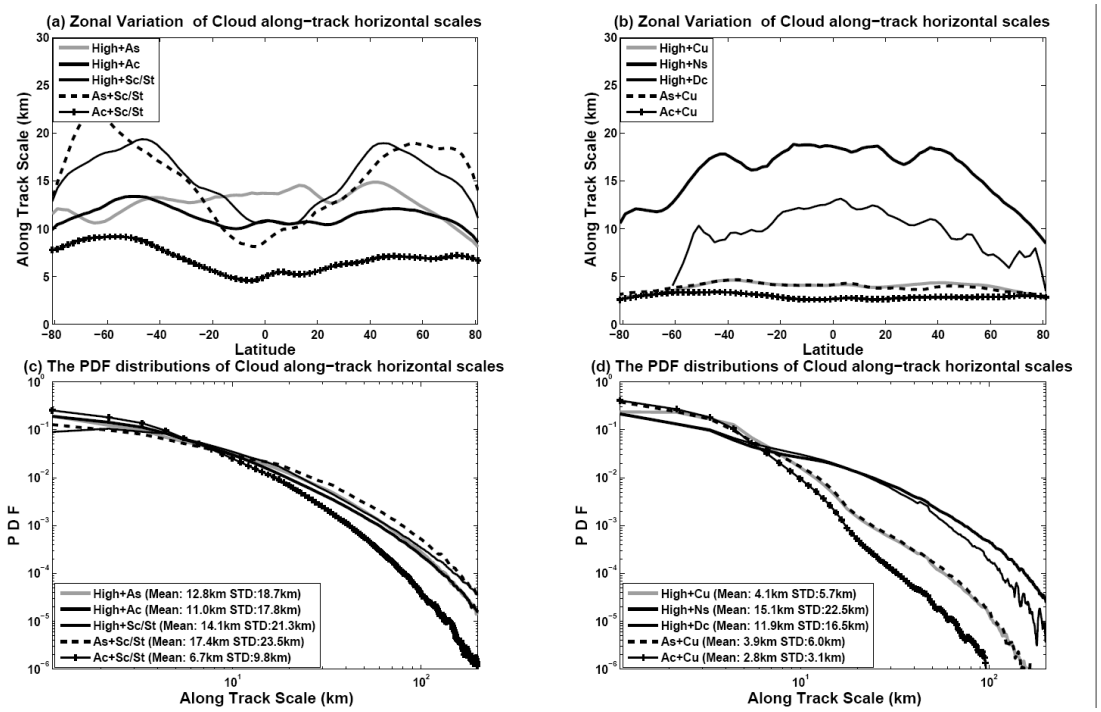

Figure 4. (a)-(b):The zonal variation of cloud along-track horizontal scales for these multilayered cloud systems and (c)-(d): their probability distribution.

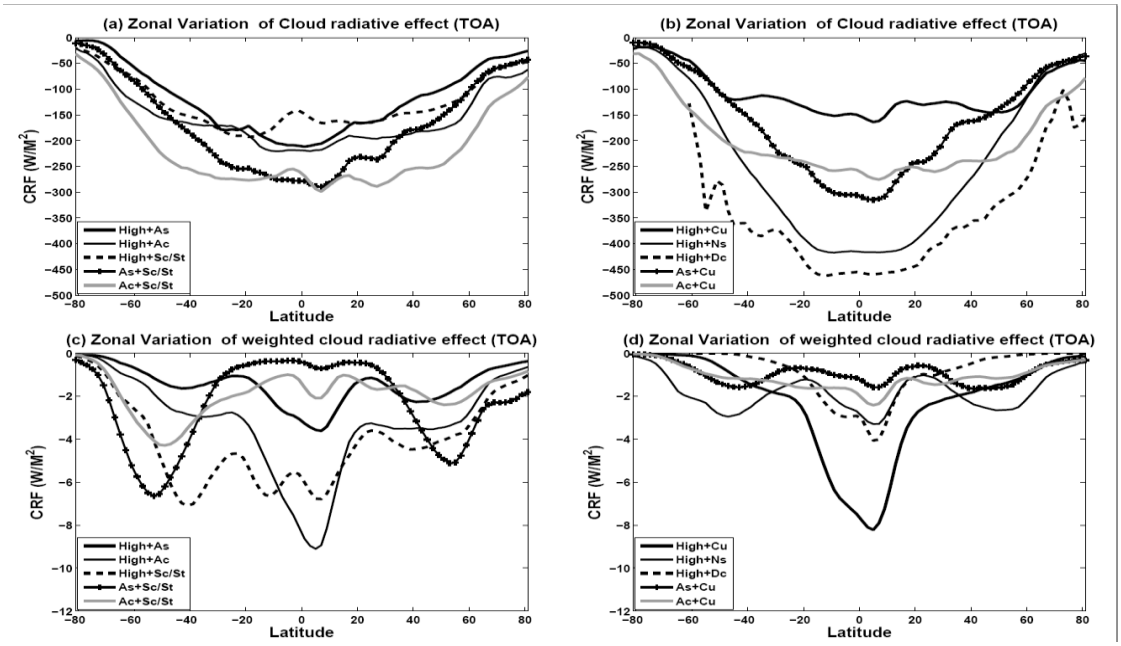

Figure 5. (a)-(d):The zonal distributions of instantaneous net cloud radiative effect and weighted instantaneous net cloud radiative effect by considering the frequency of occurrence of each cloud type for different multilayered cloud systems at the top of atmosphere (TOA) during daytime (that is, overpass time of satellite).

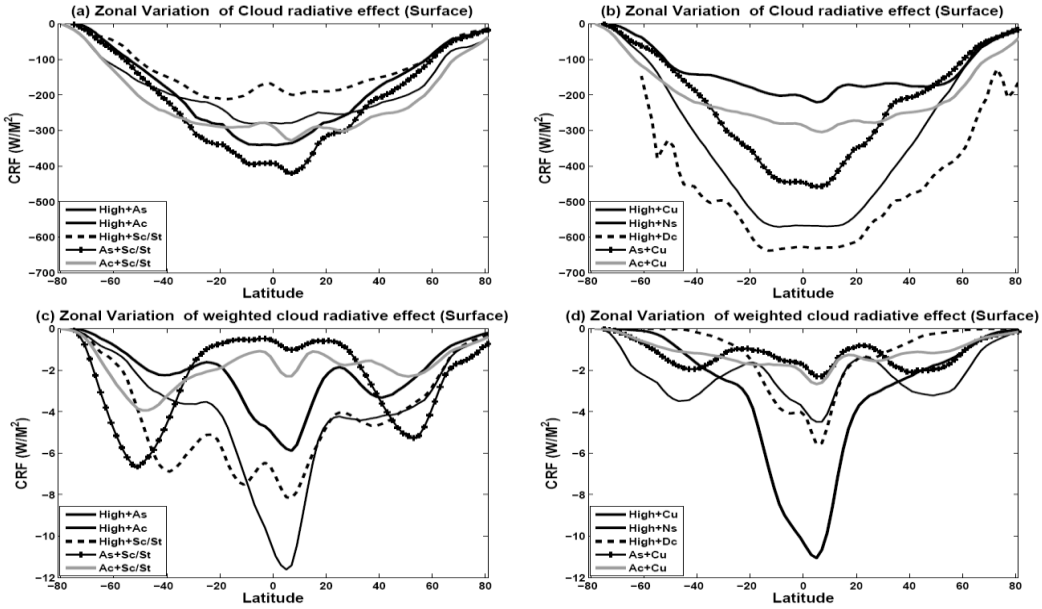

Figure 6. Same with Figure5, but at the surface during the daytime.

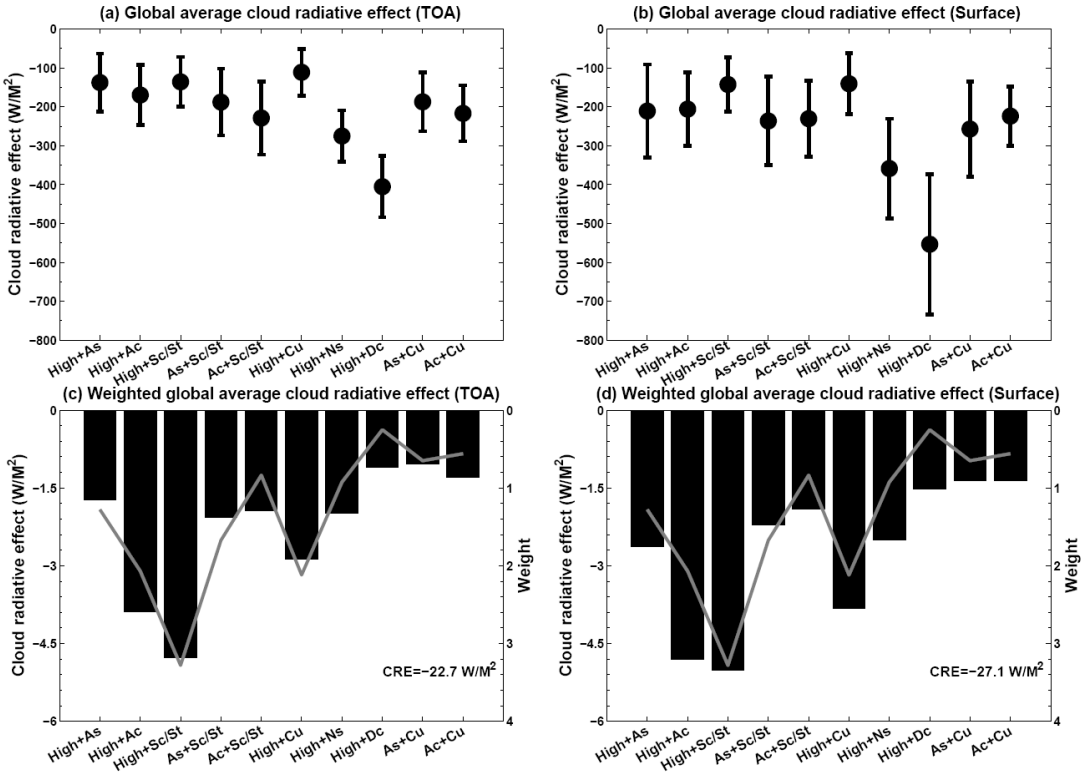

Figure 7. The global average instantaneous net cloud radiative effect and weighted instantaneous net cloud radiative effect for different multilayered cloud types at TOA and surface only during daytime. The gray line presents the global average frequency of occurrence of each cloud type only during daytime (that is, weights). The total weighted instantaneous net cloud radiative effects of ten multilayered cloud system are also showed in the figure 7c and 7d. TOA (-22.7 W/m^2); Surface (-27.1 W/m^2).

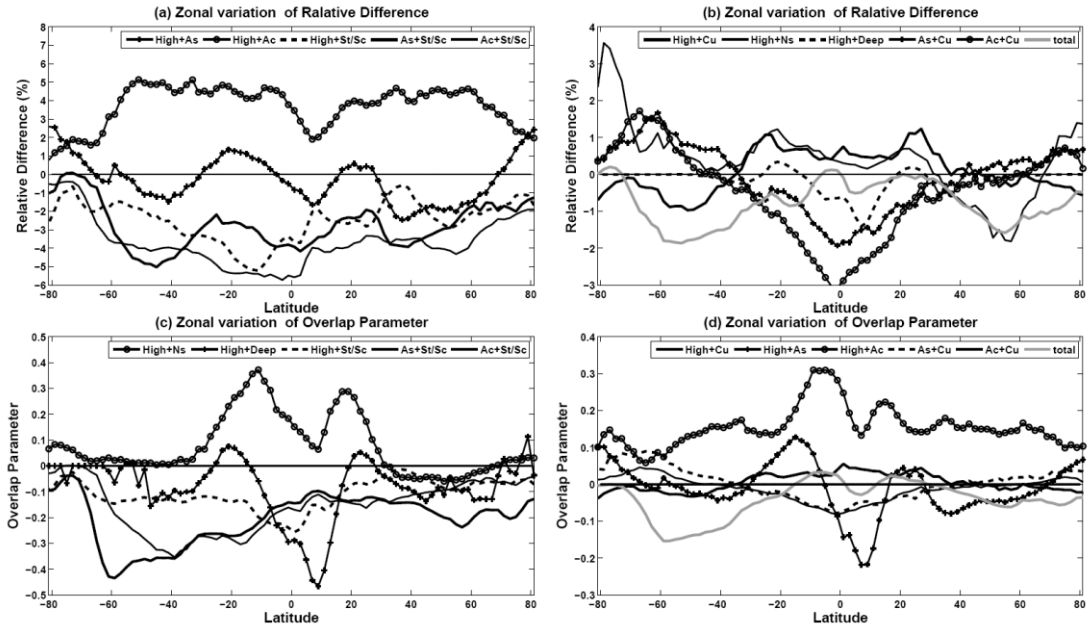

Figure 8. (a)-(b): The zonal distributions of the relative difference between the random and actual overlap for different multilayered cloud types and the cumulative relative difference of all multilayered cloud types (gray line). (c)-(d): The zonal distributions of the overlap parameter for different multilayered cloud types and the cumulative overlap parameter of all multilayered cloud types (gray line).

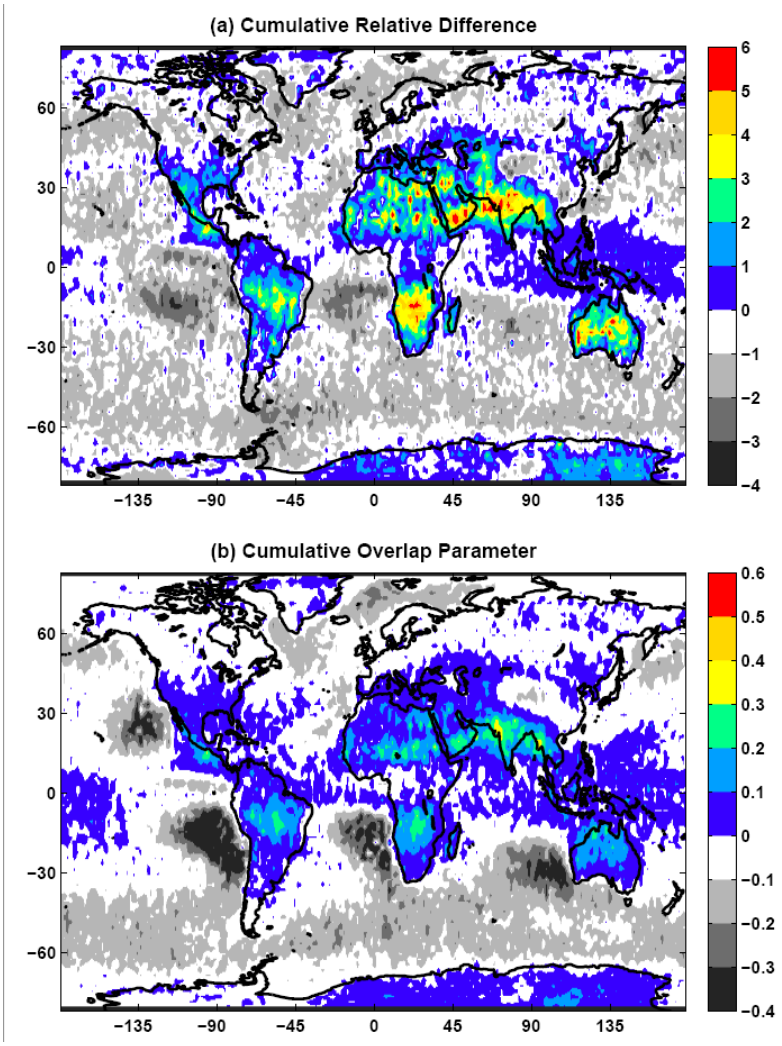

Figure 9. The global distributions of (a) the cumulative relative difference and (b) the cumulative overlap parameter of all multilayered cloud types.